IEEE Photonics Journal
An IEEE Photonics Society Publication

Open Access

Full-Vectorial Meshfree Spectral Method for Optical-Waveguide Analysis

Volume 5, Number 1, February 2013

Fahhad Alharbi

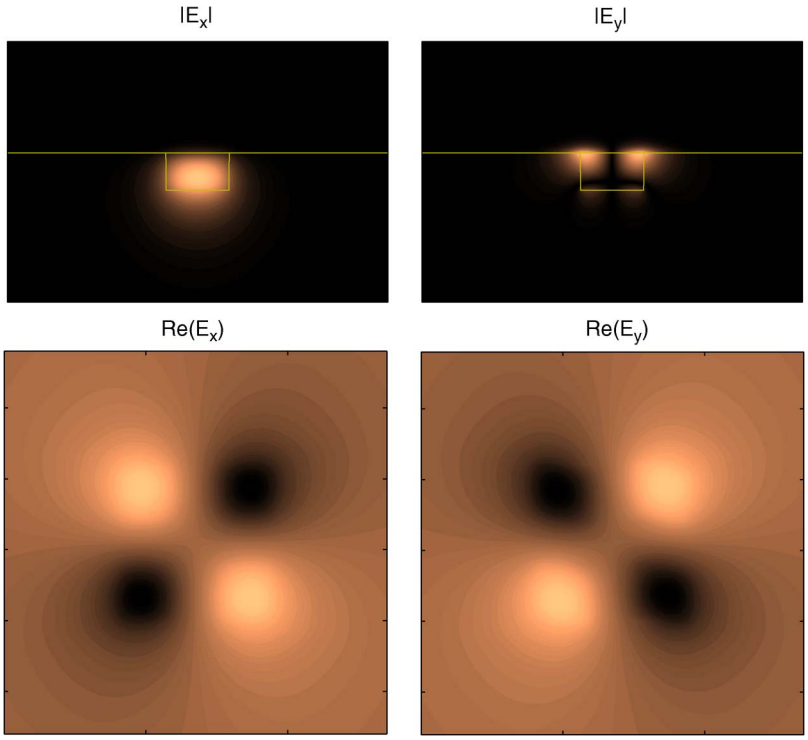

DOI: 10.1109/JPHOT.2013.2244876
1943-0655/$31.00 ©2013 IEEE

IEEE photonics SOCIETY

IEEE

Full-Vectorial Meshfree Spectral Method for Optical-Waveguide Analysis

Fahhad Alharbi

Qatar Environment and Energy Research Institute (QEERI), Doha, Qatar
King Abdulaziz City for Science and Technology (KACST), Riyadh 11442, Saudi Arabia

DOI: 10.1109/JPHOT.2013.2244876
1943-0655/$31.00 ©2013 IEEE

Manuscript received January 16, 2013; revised January 28, 2013; accepted January 28, 2013. Date of publication February 6, 2013; date of current version February 20, 2013. Corresponding author: F. Alharbi (e-mail: falharbi@qf.org.qa).

Abstract: A full-vectorial multidomain spectral method (MDSM) for optical modal analysis is developed and presented. The formulation is based on considering the coupling between the transverse magnetic (TM) field components as the other electromagnetic components can be calculated directly from them. The method is meshfree where Chebyshev polynomials are used to expand the components in the internal domains and tempered exponential sets are used for the external domains. Practically, the presented method is applicable to 3-D optical-waveguide structures that are invariant in one direction. The field profiles are expanded by 1-D preselected basis functions with variable expansion coefficients. The presented method is used to study different waveguide structures and exhibits superior performance in time and accuracy and highly agrees with the published results obtained by various methods. The presented method computations are very fast when compared with the conventional mesh-based methods. To have the same accuracy, the required number of unknowns in MDSM is orders of magnitude less than those needed by finite-difference and finite-element methods.

Index Terms: Full vectorial, optical waveguide, multidomain spectral method (MDSM), meshfree.

1. Introduction

Accurate quantitative computation has become an essential part in both academia and industry. Obviously, more requirements and demands are expected with time. As the size and the complexity of numerically studied problems grow, it becomes clear that mesh-based computational requirements are becoming expensive and prohibitive, and this leads to seeking alternatives. One of the promising emerging alternative numerical methods is multidomain spectral method (MDSM). In spectral methods (SMs), the unknown functions are approximated by expansion using a preselected basis sets. To avoid the Gibbs phenomenon, the computational window in MDSM is divided into domains where the structural parameters are essentially smooth in each domain and the discontinuities lie at the boundaries. The implementations in each domain are then joined together by applying the proper boundary conditions [1]–[4].

SMs are not new but were dominated for a long time by the versatile yet computationally expensive mesh-based finite-difference and finite-element methods (FDM/FEM). They have been used regularly in fluid dynamics and solid deformation analyses for more than two decades. Just recently, they were introduced to and used for other fields. In optoelectronics, they are used to analyze optical waveguides [3], [5]–[9], wave propagation [10], [11], quantum structures [2], [12], and photonic crystals [13]. Alharbi and Scott [3] introduced a full basis expansion MDSM

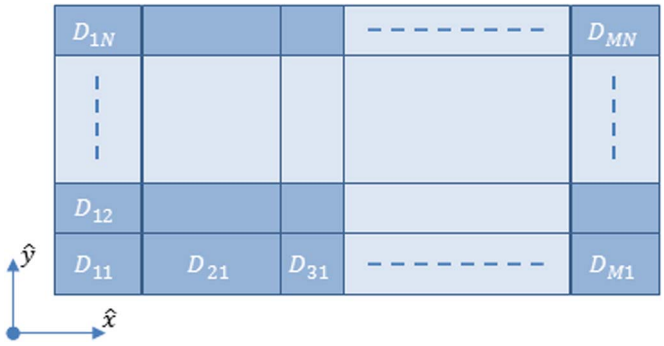

Fig. 1. Division of the structure into domains.

formulation based on mode matching, dimension reduction, and transfer matrix techniques to analyze scalar modes in optical waveguides. In this paper, the same method is extended into full-vectorial formulation.

In the next section, the mathematical foundations are presented and discussed. This is followed by the numerical formulation. Then, the presented method is applied to different optical-waveguide structures. For validation, the results are compared with published data. The comparison reveals clearly the accuracy and efficiency of the presented method. The computation is very fast when compared with the conventional mesh-based methods. To have the same accuracy, the required number of unknowns in MDSM is orders of magnitude less than those needed by FDM and FEM. Timewise, the presented method is iterative, and each iteration lasts about 20 ms and around 20 iterations are needed to have a convergence to the fifth decimal. The used basis sets are Chebyshev polynomials for bounded domains and predefined exponential sets [14] for the half-bounded domains.

2. Mathematical Foundation

2.1. The Structure

As aforementioned, this paper is an extension of a previous work, and hence, the same computational window decomposition is used and the same constraints are applied [3]. The method is applicable for 3-D structures that are invariant in one direction. This direction is assumed to be the z-axis, and this allows representing any field as follows:

$$\mathcal{F}(\mathbf{r}_\perp, z, t) = \sum_{pq} \mathbf{F}_{pq}(\mathbf{r}_\perp) e^{i(n_{\text{eff},pq} k_q z - \omega_q t)} \tag{1}$$

where $n_{\text{eff},pq}$ is the effective index of the pth mode at the angular frequency ω_q, and k_q is the free-space wavenumber at ω_q. The presented method finds the coupled electromagnetic-field (EMF) components $\mathbf{F}_{pq}$ and their corresponding effective indexes $n_{\text{eff},pq}$. Since the modes are found separately, the subscripts p and q will be omitted for the remaining of the paper.

The cross section of the structure is divided into M regions in such a way that, in each region, the structure function is invariant in another direction. Then, the regions are divided into homogeneous N layers. Fig. 1 shows how the computational window is divided into domains where the dielectric properties are constant in each domain. Cartesian coordinates are assumed and used in this paper. Any other 2-D system can be used as well.

2.2. EMF Components' Coupling and the Required Base Components

The presented method is full vectorial where it accounts for couplings between EMF components. We do not need to solve for all the six EMF components simultaneously to account for these

couplings. From Maxwell's equations in source-free nonmagnetic medium

$$\nabla \times \mathbf{E} = i\omega\mu_0 \mathbf{H} \tag{2}$$

$$\nabla \times \mathbf{H} = -i\omega\varepsilon_0 n^2 \mathbf{E} \tag{3}$$

where **E** is the electric field, **H** is the magnetic field, μ_0 is the free-space permeability, and n is the complex refractive index. It is clear that, if the **E** components (E_x, E_y, E_z) are known, the **H** components (H_x, H_y, H_z) can be calculated straightforwardly and vice versa. So to account for coupling, either the three electric or the three magnetic components can be used as the base components. Furthermore, this can be reduced further into two base components only for modal analysis. From the last of Maxwell's equations in source-free medium (Gauss's law for magnetism)

$$\nabla \cdot \mathbf{H} = 0 \tag{4}$$

and from the field form (1), which implies that, for each mode

$$\frac{\partial}{\partial z} = i n_{\text{eff}} k_0 \tag{5}$$

$$\frac{\partial^2}{\partial z^2} = -n_{\text{eff}}^2 k_0^2 \tag{6}$$

it can be shown that (4) is reduced to

$$\frac{\partial H_x}{\partial x} + \frac{\partial H_y}{\partial y} + i n_{\text{eff}} k_0 H_z = 0. \tag{7}$$

Therefore, if H_x and H_y are known, H_z can be calculated straightforwardly. The same thing can be applied as well to the **E** components. In this paper, H_x and H_y are used as the base components.

2.3. Governing Equation and Boundary Conditions

Since each domain is homogeneous, the governing equation within each domain, which is based on harmonic wave expansion for any EMF component, is simply Helmholtz equation. By applying the harmonic solution form (1) for each mode, the governing wave equation for the *mn*th domain becomes

$$\frac{\partial^2 H_\eta^{(mn)}}{\partial x^2} + \frac{\partial^2 H_\eta^{(mn)}}{\partial y^2} + k_0^2 \left(\varepsilon^{(mn)} - n_{\text{eff}}^2\right) H_\eta^{(mn)} = 0 \qquad \begin{matrix} 1 \le m \le M \\ 1 \le n \le N \end{matrix} \tag{8}$$

where $\varepsilon^{(mn)}$ is the dielectric constant in the *mn*th domain, and η is either x or y.

Within each region, the boundary conditions of the base components and its first derivative are applied across the horizontal interfaces. The domain above any horizontal line is denoted by n (from north), and the one below it is denoted by s (from south). For the base components, since the presented formulation is developed for nonmagnetic medium, they are continuous. So

$$H_x|_n = H_x|_s \tag{9}$$

$$H_y|_n = H_y|_s. \tag{10}$$

For the first derivative conditions, the continuity of H_z and E_z are applied. From (7), it is clear that

$$-i n_{\text{eff}} k_0 H_z = \frac{\partial H_x}{\partial x} + \frac{\partial H_y}{\partial y}.$$

So

$$\frac{\partial H_x}{\partial x}|_n + \frac{\partial H_y}{\partial y}|_n = \frac{\partial H_x}{\partial x}|_s + \frac{\partial H_y}{\partial y}|_s. \tag{11}$$

Also, from (3), it can be shown that

$$-i\omega\varepsilon_0\varepsilon^{(mn)}E_z = \frac{\partial H_y}{\partial x} - \frac{\partial H_x}{\partial y}.$$

So

$$\frac{1}{\varepsilon^{(mn+1)}}\left[\frac{\partial H_y}{\partial x}|_n - \frac{\partial H_x}{\partial y}|_n\right] = \frac{1}{\varepsilon^{(mn)}}\left[\frac{\partial H_y}{\partial x}|_s - \frac{\partial H_x}{\partial y}|_s\right]. \tag{12}$$

The vertical interfaces conditions are considered next. By considering the used structure decomposition, each domain is set to interface with at least one another domain along the x-axis. These domains are matched in their vertical extensions. So, the domain to the left of any vertical line is denoted by w from west, and the one to the right it is denoted by e from east.

For the base components, since the presented formulation is developed for nonmagnetic medium, the magnetic-field components are continuous. So

$$H_x|_w = H_x|_e \tag{13}$$
$$H_y|_w = H_y|_e. \tag{14}$$

Also, the continuity of H_z and E_z are applied for the first derivative conditions. So

$$\frac{\partial H_x}{\partial x}|_w + \frac{\partial H_y}{\partial y}|_w = \frac{\partial H_x}{\partial x}|_e + \frac{\partial H_y}{\partial y}|_e \tag{15}$$
$$\frac{1}{\varepsilon^{(mn)}}\left[\frac{\partial H_y}{\partial x}|_w - \frac{\partial H_x}{\partial y}|_w\right] = \frac{1}{\varepsilon^{(m+1n)}}\left[\frac{\partial H_y}{\partial x}|_e - \frac{\partial H_x}{\partial y}|_e\right]. \tag{16}$$

3. Numerical Formulation

3.1. Basis Sets and Moments Matrices

In the mnth domain, the base components H_x and H_y are expanded as follows:

$$H_x^{(mn)} = \sum_l c_x^{(mnl)}(x)P_{nl}(y) \tag{17}$$
$$H_y^{(mn)} = \sum_l c_y^{(mnl)}(x)P_{nl}(y) \tag{18}$$

where P_{nl} is the preselected basis set. The basis set is independent of the region as the same set is used in all the horizontally adjacent domains. In this paper, Chebyshev polynomials are used for bounded domains, and the preselected basis sets are used for half-bounded domains [14]. To match the real dimensions with the basis sets' spaces, direct linear coordinate transformation is used. $c_x^{(mnl)}$ and $c_y^{(mnl)}$ are the unknown expansion coefficients, and they are set as functions of x.

Based on this expansion form, the following matrices are defined and will be reused routinely in the remaining of the paper. They are defined according to their scalar product elements

$$\mathbf{S}_n = [S_{nkl}] \qquad S_{nkl} = \left(P_{nk}(y)\left|w(y)\frac{d^2}{dy^2}\right|P_{nl}(y)\right) \tag{19}$$
$$\mathbf{F}_n = [F_{nkl}] \qquad F_{nkl} = \left(P_{nk}(y)\left|w(y)\frac{d}{dy}\right|P_{nl}(y)\right) \tag{20}$$
$$\mathbf{Z}_n = [Z_{nkl}] \qquad Z_{nkl} = (P_{nk}(y)|w(y)|P_{nl}(y)) \tag{21}$$

where $w(y)$ is the weight function associated with the selected basis sets. For Chebyshev basis set of the first kind polynomials, it is $1/\sqrt{1-y^2}$, while it is $\sqrt{1-y^2}$ for Chebyshev basis set of the second kind polynomials. For the predefined exponential basis set, the weight function is just 1.

3.2. MDSM Implementation

By applying the expansion forms [(17), (18)] in the governing wave equation (8), it becomes

$$\sum_l \frac{d^2 c_x^{(mnl)}(x)}{dx^2} P_{nl}(y) + \sum_l c_x^{(mnl)}(x) \frac{d^2 P_{nl}(y)}{dy^2} + k_0^2 \left(\varepsilon^{(mn)} - n_{\text{eff}}^2\right) \sum_l c_x^{(mnl)}(x) P_{nl}(y) = 0 \tag{22}$$

for H_x and

$$\sum_l \frac{d^2 c_y^{(mnl)}(x)}{dx^2} P_{nl}(y) + \sum_l c_y^{(mnl)}(x) \frac{d^2 P_{nl}(y)}{dy^2} + k_0^2 \left(\varepsilon^{(mn)} - n_{\text{eff}}^2\right) \sum_l c_y^{(mnl)}(x) P_{nl}(y) = 0 \tag{23}$$

for H_y. By calculating the scalar products using the same basis set, the above two equation can be represented by the following matrix form:

$$\mathbf{Z}_n \frac{d^2 \mathbf{c}_\eta^{(mn)}}{dx^2} + \left[k_0^2 \left(\varepsilon^{(mn)} - n_{\text{eff}}^2\right) \mathbf{Z}_n + \mathbf{S}_n\right] \mathbf{c}_\eta^{(mn)} = \mathbf{Z}_n \frac{d^2 \mathbf{c}_\eta^{(mn)}}{dx^2} + \mathbf{G}_n \mathbf{c}_\eta^{(mn)} = \mathbf{0} \tag{24}$$

where $\mathbf{c}_x^{(mn)}$ is the combining vector of the expansion coefficients $c_x^{(mnl)}$

$$\mathbf{c}_\eta^{(mn)} = \left[c_\eta^{(mn1)} c_\eta^{(mn2)} \cdots c_\eta^{(mnL_{mn})}\right]^T. \tag{25}$$

Then, the wave equation of all the layers (of the above form) in the mth region are combined in one general equation as follows:

$$\mathbf{Z} \frac{d^2 \mathbf{c}^{(m)}}{dx^2} + \mathbf{G} \mathbf{c}^{(m)} = \mathbf{0} \tag{26}$$

where

$$\mathbf{Z} = \text{diag}(\mathbf{Z}_1, \mathbf{Z}_2, \ldots, \mathbf{Z}_N, \mathbf{Z}_1, \mathbf{Z}_2, \ldots, \mathbf{Z}_N) \tag{27}$$

$$\mathbf{G} = \text{diag}(\mathbf{G}_1, \mathbf{G}_2, \ldots, \mathbf{G}_N, \mathbf{G}_1, \mathbf{G}_2, \ldots, \mathbf{G}_N) \tag{28}$$

$$\mathbf{c}^{(m)} = \begin{bmatrix} \mathbf{c}_x^{(m1)} \\ \mathbf{c}_x^{(m2)} \\ \vdots \\ \mathbf{c}_x^{(mN)} \\ \mathbf{c}_y^{(m1)} \\ \mathbf{c}_y^{(m2)} \\ \vdots \\ \mathbf{c}_y^{(mN)} \end{bmatrix}. \tag{29}$$

Then, the horizontal interfaces conditions are applied. By using the expansion forms, i.e., (9) and (10), the boundary conditions become

$$\sum_l c_x^{(mnl)}(x) P_{nl}(y_n) = \sum_l c_x^{(mn+1l)}(x) P_{n+1l}(y_n) \tag{30}$$

$$\sum_l c_y^{(mnl)}(x) P_{nl}(y_n) = \sum_l c_y^{(mn+1l)}(x) P_{n+1l}(y_n) \tag{31}$$

$$\sum_l \frac{dc_x^{(mnl)}}{dx} P_{nl}(y_n) + \sum_l c_y^{(mnl)}(x) \frac{dP_{nl}}{dy}(y_n)$$

$$= \sum_l \frac{dc_x^{(mn+1l)}}{dx} P_{n+1l}(y_n) + \sum_l c_y^{(mn+1l)}(x) \frac{dP_{n+1l}}{dy}(y_n) \tag{32}$$

$$\frac{1}{\varepsilon^{(mn)}} \left[\sum_l c_x^{(mnl)}(x) \frac{dP_{nl}}{dy}(y_n) - \sum_l \frac{dc_y^{(mnl)}}{dx} P_{nl}(y_n) \right]$$

$$= \frac{1}{\varepsilon^{(mn+1)}} \left[\sum_l c_x^{(mn+1l)}(x) \frac{dP_{n+1l}}{dy}(y_n) - \sum_l \frac{dc_y^{(mn+1l)}}{dx} P_{n+1l}(y_n) \right] \tag{33}$$

where y_n is the transformed y-axis real space value and the interface between the mnth and $m(n+1)$th domains in the mth region. This is applied to all the horizontal interfaces at the mth region. The resulted equations can be combined in the following matrix form:

$$\mathbf{B}_f^{(m)} \frac{d\mathbf{c}^{(m)}}{dx} + \mathbf{B}_z^{(m)} \mathbf{c}^{(m)} = \mathbf{0}. \tag{34}$$

Equations (26) and (34) are then combined in the following equation:

$$\begin{bmatrix} \mathbf{Z} \\ \mathbf{0} \end{bmatrix} \frac{d^2\mathbf{c}^{(m)}}{dx^2} + \begin{bmatrix} \mathbf{0} \\ \mathbf{B}_f^{(m)} \end{bmatrix} \frac{d\mathbf{c}^{(m)}}{dx} + \begin{bmatrix} \mathbf{G} \\ \mathbf{B}_z^{(m)} \end{bmatrix} \mathbf{c}^{(m)} = \mathbf{0}. \tag{35}$$

This differential system is overdetermined and can be solved by different approaches such as Tau method [4], least square [15], QR decomposition, and minimal perturbation [16]. In this paper, Tau approach is used in which the system matrices are squared by omitting some of the less populated rows that are not related to the boundary conditions. This reduces the rank of the matrices, and hence, the solutions are based on reduced sets of eigenpairs. They take the following form:

$$\mathbf{c}^{(m)}(x) = \mathbf{R}_m^f e^{\Lambda_m^f (x - x_m)} \mathbf{f}_m + \mathbf{R}_m^b e^{\Lambda_m^b (x - x_{m+1})} \mathbf{b}_m \tag{36}$$

where Λ_m^f (Λ_m^b) and $\mathbf{R}_m^f$ ($\mathbf{R}_m^b$) are the forward (backward) traveling eigenvalues and their corresponding eigenvectors matrices. Eigenvalues are arranged as forward and backward traveling to ensure that the exponentials are diverging. The only unknowns in this solution are $\mathbf{f}_m$ and $\mathbf{b}_m$. These shall be found later by applying vertical boundary and initial conditions.

As done in the original scalar formulation [3], the wave equation is solved in each region separately but with variable projection vectors since the initial conditions (of each region) are not applied yet. These initial conditions are applied later by considering the vertical interfaces between the regions and the fact that, for spatial modal analysis, the desired solutions are bounded for nonperiodic structures. This implies that no forward-traveling eigenvector in the first region or backward-traveling eigenvector in the last region exist. Then, the solution in each region is obtained completely.

The next step is to consider the vertical interfaces boundary conditions. They involved the base components and their derivative with respect to x. The conditions between adjacent domains were presented earlier, and by applying them and the expansion forms at $x = x_{m+1}$, which is the interface between the mth and $(m+1)$th regions, we get

$$\sum_l c_x^{(mnl)}(x_{m+1}) P_{nl}(y) = \sum_l c_x^{(m+1nl)}(x_{m+1}) P_{nl}(y) \tag{37}$$

$$\sum_l c_y^{(mnl)}(x_{m+1}) P_{nl}(y) = \sum_l c_y^{(m+1nl)}(x_{m+1}) P_{nl}(y) \tag{38}$$

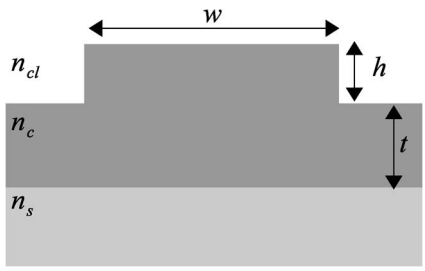

Fig. 2. Rib waveguide geometry.

$$\sum_l \left.\frac{dc_x^{(mnl)}}{dx}\right|_{x=x_{m+1}} P_{nl}(y) + \sum_l c_y^{(mnl)}(x_{m+1})\frac{dP_{nl}}{dy}(y) = \sum_l \left.\frac{dc_x^{(m+1nl)}}{dx}\right|_{x=x_{m+1}} P_{nl}(y) + \sum_l c_y^{(m+1nl)}(x_{m+1})\frac{dP_{nl}}{dy}(y) \tag{39}$$

$$\frac{1}{\varepsilon^{(mn)}}\left[\sum_l c_x^{(mnl)}(x_{m+1})\frac{dP_{nl}}{dy} - \sum_l \frac{dc_y^{(mnl)}}{dx}|_{x=x_{m+1}} P_{nl}(y)\right] = \frac{1}{\varepsilon^{(m+1n)}}\left[\sum_l c_x^{(m+1nl)}(x_{m+1})\frac{dP_{nl}}{dy} - \sum_l \left.\frac{dc_y^{(m+1nl)}}{dx}\right|_{x=x_{m+1}} P_{nl}(y)\right]. \tag{40}$$

By calculating the scalar products using the same basis set, rearranging the resulted equations in matrix form, and combining the equations of all the domains around $x = x_{m+1}$, the above equations become

$$\mathbf{W}_m \mathbf{c}^{(m)}(x_{m+1}) = \mathbf{W}_{m+1}\mathbf{c}^{(m+1)}(x_{m+1}) \tag{41}$$

$$\mathbf{T}_m \left.\frac{d\mathbf{c}^{(m)}}{dx}\right|_{x=x_{m+1}} + \mathbf{U}_m \mathbf{c}^{(m)}(x_{m+1}) = \mathbf{T}_{m+1}\left.\frac{d\mathbf{c}^{(m+1)}}{dx}\right|_{x=x_{m+1}} + \mathbf{U}_{m+1}\mathbf{c}^{(m+1)}(x_{m+1}). \tag{42}$$

Afterward, the same procedure used in the previous work for scalar field [3] is used with minor modification to include the $\mathbf{U}_m$ matrices to link the solutions in all the regions. The same technique is also used to find the effective indexes n_{eff} and their corresponding vectors. We refer the reader to that paper for the details.

4. Results and Discussion

4.1. Rib Waveguide

The first structure to be analyzed is of rib waveguide geometry, which is one of the geometries that are widely used in optical devices (see Fig. 2), and it is routinely used to compare and validate numerical methods. The parameters of the first studied rib waveguide are shown in Table 1. This structure has been studied heavily for numerical methods comparisons [5], [17]–[28].

Tables 2 and 3 show the results obtained for both quasi-transverse electric (TE) and quasi-TM fundamental modes, respectively, by this paper (see Fig. 3) and various full-vectorial methods; namely, FDM [24], [26], FEM [28], hybrid FDM, and beam propagation method (BPM) [22], mode matching method (MMM) [27], [28], and multidomain pseudospectral frequency domain (PSFD) [5]. The results are presented by the normalized propagation constant β, where

$$\beta = \frac{n_{\text{eff}}^2 - n_{\text{clad}}^2}{n_{\text{core}}^2 - n_{\text{clad}}^2} \tag{43}$$

TABLE 1

Used rib waveguide parameters with varied rib height

$\lambda\ (\mu m)$	n_s	n_c	n_{cl}	$h\ (\mu m)$	$h+t\ (\mu m)$	$w\ (\mu m)$
1.15	3.40	3.44	1.0	0.1:0.9	1.0	3.0

TABLE 2

Quasi-TE modes' normalized propagation constants for the first studied rib waveguides (Table 1) obtained by the presented full vectorial method (FV-MDSM) and the previous scalar version and other full vectorial methods

$h\ (\mu m)$	FV-MDSM	Sc. MDSM [3]	FDM [24]	FDM [26]	FEM [28]	FD-BPM [22]	MMM [27]	MMM [28]
0.1	0.3017159279	0.301975	0.30200	0.30280	0.30188	0.30390	0.30190	0.30191
0.2	0.3057570287		0.30500					
0.3	0.3106461897	0.311182	0.31100	0.31180	0.31099	0.31440	0.31100	0.03110
0.4	0.3181465960		0.31700					
0.5	0.3270323325	0.326658	0.32600	0.32770	0.32697	0.33030	0.32700	0.32702
0.6	0.3380259816		0.33700					
0.7	0.3516051841	0.350679	0.35000	0.35150	0.35117	0.35330	0.35100	0.35118
0.8	0.3670332632		0.36700					
0.9	0.3882784476	0.387979	0.38800	0.38860	0.38790	0.38830		

TABLE 3

Quasi-TM modes' normalized propagation constants for the first studied rib waveguides (Table 1) obtained by the presented full vectorial method (FV-MDSM) and the previous scalar version and other full vectorial methods

$h\ (\mu m)$	FV-MDSM	Sc. MDSM [3]	PSFD [5]	FDM [26]	FEM [28]	FD-BPM [22]	MMM [27]	MMM [28]
0.1	0.2674743256	0.267387	0.2674483	0.26780	0.26745	0.26900	0.26740	0.26745
0.2	0.2706445487		0.2706354					
0.3	0.2745399487	0.274976	0.2751333	0.27540	0.27508	0.27760	0.27510	0.27513
0.4	0.2810203433		0.2811860					
0.5	0.2884805600	0.288714	0.2889903	0.28930	0.28890	0.29150	0.28900	0.28899
0.6	0.2983865400		0.2987316					
0.7	0.3106991823	0.310351	0.3106792	0.31090	0.31063	0.31270	0.31070	0.31070
0.8	0.3256274210							
0.9	0.3470709715	0.345431		0.34560	0.34510	0.34550		

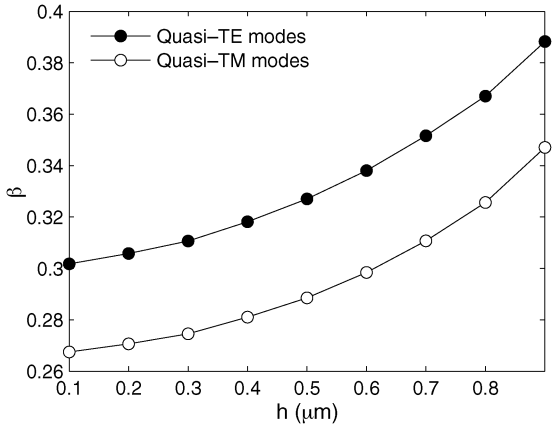

Fig. 3. Normalized propagation constant β of the fundamental quasi-TE and quasi-TM modes supported by the first studied rib waveguide as a function of the rib height *h*.

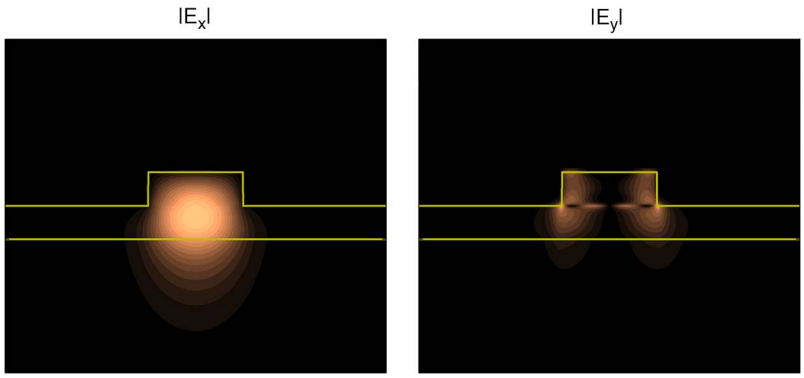

Fig. 4. Profiles of $|H_x|$ and $|H_y|$ of the fundamental quasi-TE mode supported by the first studied rib waveguide for $t = h = 0.5$ μm.

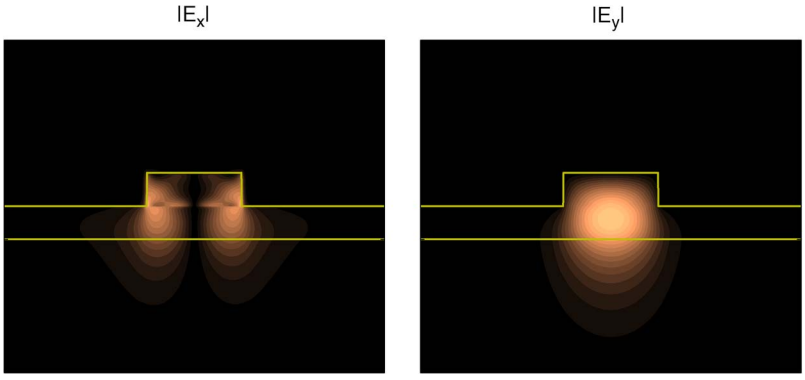

Fig. 5. Profiles of $|H_x|$ and $|H_y|$ of the fundamental quasi-TM mode supported by the first studied rib waveguide for $t = h = 0.5$ μm.

varies between 0 and 1 based on the relevant refractive indexes n_{core} and n_{clad}. The results for both modes agree remarkably and prove the validity and high accuracy of the presented method. In the MDSM analysis, Chebyshev bases to the sixth order are used in the inertial layers, and tempered exponential basis sets (13 bases) [14], [29] are used in the external layers. In Fig. 2, β of the fundamental modes is shown as a function of the rib height h. Obviously, as h increases, the modes will have mode area to occupy in the core layer, and hence, β increases with h. Figs. 4 and 5 show the profiles of $|H_x|$ and $|H_y|$ for both fundamental quasi-TE and quasi-TM modes, respectively for $t = h = 0.5$ μm.

Another rib waveguide is studied also to check the convergence. So, $\beta_{\text{eff}}^{\text{TE}}$ (see Fig. 6) and $\beta_{\text{eff}}^{\text{TM}}$ (see Fig. 7) are plotted as functions of N (where N is the number of unknowns for every EMF base component) and make a comparison with the results obtained using FDM [30], FEM [28], and MMM [28]. The parameters of the studied rib waveguide are shown in Table 4, and the extrapolated values are shown as red lines. It is clear that all the methods converge. However, MMM and the presented MDSM, which are both meshfree, result in considerably faster convergence when compared with FDM and FEM.

4.2. Buried Channel Waveguide

The second structure to be studied is the buried channel waveguide, which is shown in Fig. 8 at 1.55-μm wavelength. For this structure, the calculated n_{eff} are 1.510676 for the fundamental quasi-TE mode and 1.507918 for the fundamental quasi-TM mode. The profiles of these modes are shown in Figs. 9 and 10, respectively.

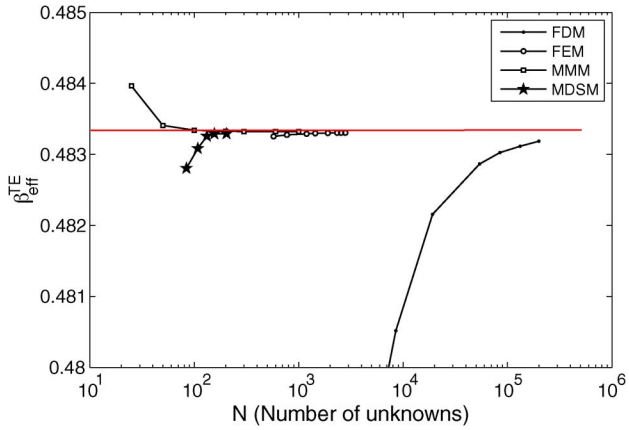

Fig. 6. β_{eff}^{TE} versus N as obtained by this paper, FDM [30], FEM [28], and MMM [28]. The extrapolated value is shown as a red line.

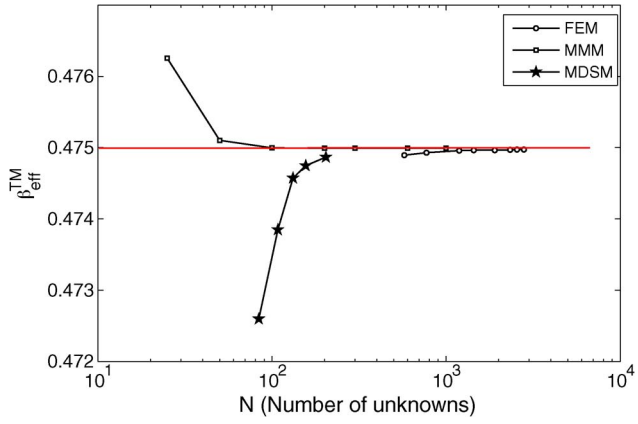

Fig. 7. β_{eff}^{TM} versus N as obtained by this paper, FEM [28], and MMM [28]. The extrapolated value is shown as a red line.

TABLE 4

Used rib waveguide parameters with varied rib height

$\lambda\ (\mu m)$	n_s	n_c	n_{cl}	$h\ (\mu m)$	$t\ (\mu m)$	$w\ (\mu m)$
1.55	3.34	3.44	1.0	1.1	0.2	2.0

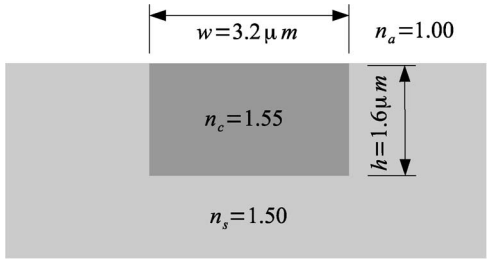

Fig. 8. Structure of the first studied buried channel waveguide.

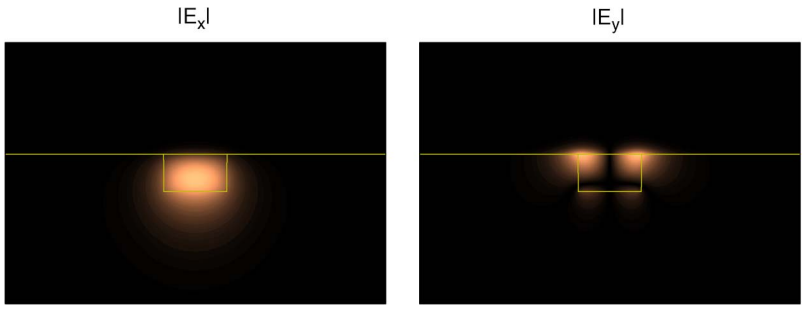

Fig. 9. Profiles of $|H_x|$ and $|H_y|$ of the fundamental quasi-TE mode supported by the studied buried channel waveguide.

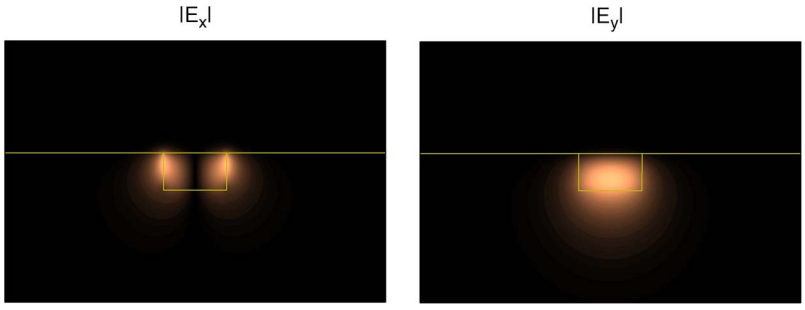

Fig. 10. Profiles of $|H_x|$ and $|H_y|$ of the fundamental quasi-TM mode supported by the first studied buried channel waveguide.

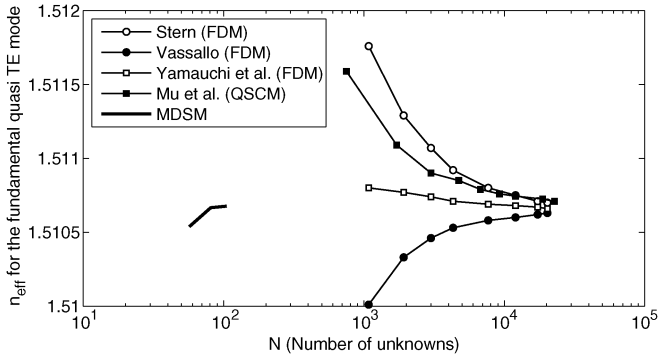

Fig. 11. n_{eff} of the fundamental quasi-TE mode versus N as obtained by this paper, FDM [19], [23], [31], QSCM [32].

To check the convergence, n_{eff} for the fundamental quasi-TE mode are plotted as functions of N (see Fig. 11) and make a comparison with the results obtained using FDM [19], [23], [31] and quadratic spline collocation (QSCM) [32]. It is clear that MDSM results in better convergence (two orders of magnitude) when compared with the other approaches.

4.3. Three-Dimensional Coupler

The last studied structure is a 3-D coupler (see Fig. 12). It was studied using various methods by Ivanova *et al.* [17]. The structure parameters are $w = 4$ μm, $h = 3$ μm, $n_s = 1.506$, and $n_c = 1.512$ at 1.32-μm wavelength.

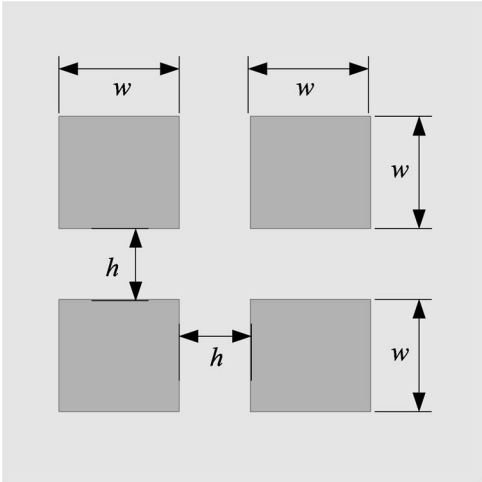

Fig. 12. Structure of the studied 3-D coupler.

TABLE 5

Effective indexes of the highest quasi-TE modes for the studied 3-D coupler waveguides obtained by the presented method and various previously published methods [17]

The method	TE00	TE01	TE10	TE11
FEM	1.5075807	1.5067966	1.5067966	1.5060260
WMM	1.5078966	1.5071085	1.5071092	1.5064697
SIM	1.5080433	1.5072134	1.5075570	1.5067277
VM-1	1.5077912	1.5069894	1.5069690	1.5061836
VM-2	1.5078853	1.5070795	1.5070793	1.5062961
Scalar MDSM	1.50787446	1.50706768	1.50706713	1.50628423
Vectorial MDSM	1.50787736	1.50706782	1.50706782	1.50628535

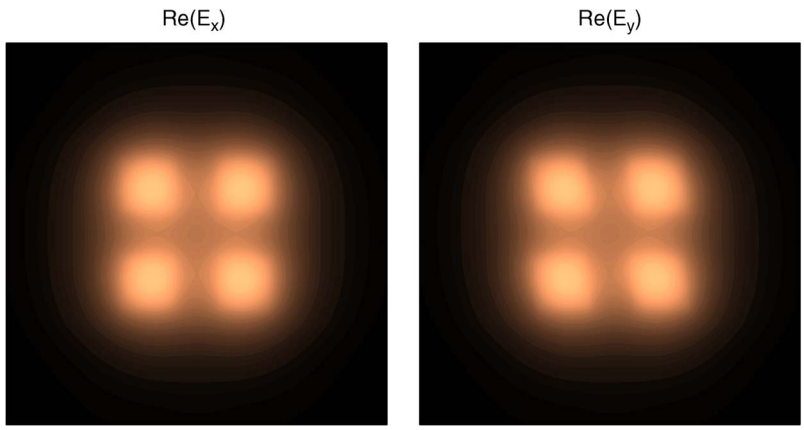

Fig. 13. Real part of the amplitudes of the obtained quasi-TE00 mode in the studied 3-D coupler.

Table 5 shows the quasi-TE effective indexes for the studied 3-D coupler waveguide as obtained by full-vectorial and scalar MDSM methods and by the various methods used by Ivanova *et al.* [17]. As can be observed, the results of the different methods highly agree with each other. In MDSM

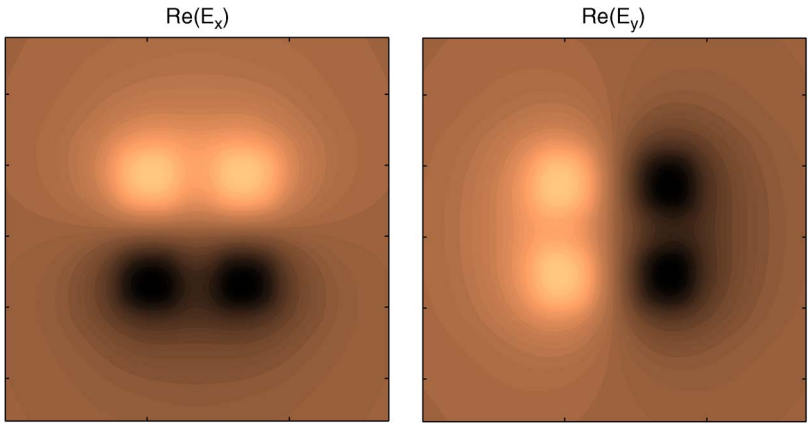

Fig. 14. Real part of the amplitudes of the obtained quasi-TE01 mode in the studied 3-D coupler.

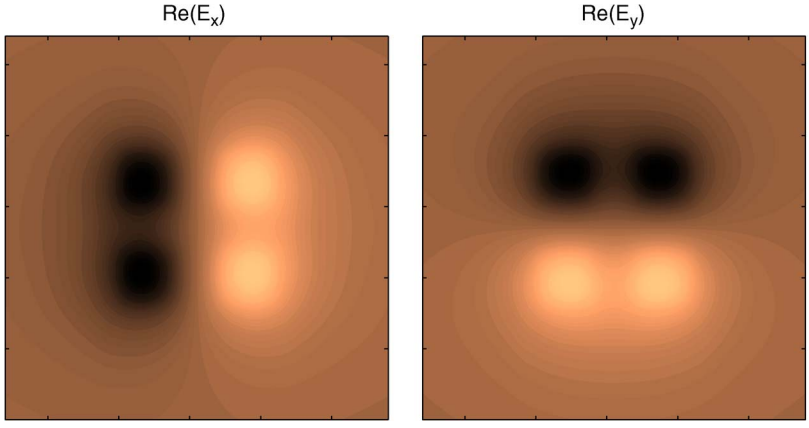

Fig. 15. Real part of the amplitudes of the obtained quasi-TE10 mode in the studied 3-D coupler.

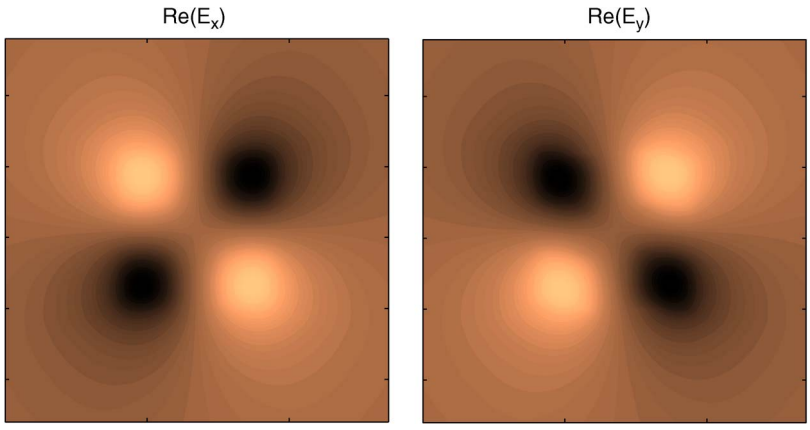

Fig. 16. Real part of the amplitudes of the obtained quasi-TE11 mode in the studied 3-D coupler.

analysis, five layers are used with eight bases in each layer. The calculated n_{eff} values for all the modes converge to the sixth decimal place. In Figs. 13–16, the real part of the amplitudes of the obtained quasi-TE modes is shown.

5. Conclusion

A new and efficient full-vectorial MDSM for optical modal analysis has been developed and presented in this paper. The formulation has been based on considering the coupling between the TM-field components as the other electromagnetic components can be calculated directly from them. The method is meshfree where Chebyshev polynomials have been used to expand the components in the internal domains and tempered exponential sets have been used for the external domains. Practically, the presented method is applicable to 3-D optical-waveguide structures that are invariant in one direction. The field profiles are expanded by 1-D preselected basis functions with variable expansion coefficients.

The presented method has been used to study different waveguide structures and exhibits superior performance in time and accuracy and highly agrees with the published results obtained by various methods. The presented method computations are very fast when compared with the conventional mesh-based methods. To have the same accuracy, the required number of unknowns in MDSM is orders of magnitude less than those needed by FDM and FEM. The same fast convergence has been also obtained using MMM method [27], [28]. This is a feature of meshfree-modal-expansion methods.

References

[1] C. Canuto, M. Hussaini, A. Quarteroni, and T. Zang, *Spectral Methods Fundamentals in Single Domains, Scientific Computation*. Berlin, Germany: Springer-Verlag, 2006.

[2] F. Alharbi, "Meshfree eigenstate calculation of arbitrary quantum well structures," *Phys. Lett. A*, vol. 374, no. 25, pp. 2501–2505, May 2010.

[3] F. Alharbi and J. Scott, "Multi-domain spectral method for modal analysis of optical waveguide," *Opt. Quantum Electron.*, vol. 41, no. 8, pp. 583–597, Jun. 2009.

[4] P. Grandclément and J. Novak, "Spectral methods for numerical relativity," *Living Rev. Rel.*, vol. 12, no. 1, pp. 1–107, Jan. 2009.

[5] P.-J. Chiang, C.-L. Wu, C.-H. Teng, C.-S. Yang, and H.-C. Chang, "Full-vectorial optical waveguide mode solvers using multidomain pseudospectral frequency-domain (PSFD) formulations," *IEEE J. Quantum Electron.*, vol. 44, no. 1, pp. 56–66, Jan. 2008.

[6] C. Huang, C. Huang, and J. Yang, "A full-vectorial pseudospectral modal analysis of dielectric optical waveguides with stepped refractive index profiles," *IEEE J. Sel. Topics Quantum Electron.*, vol. 11, no. 2, pp. 457–465, Mar./Apr. 2005.

[7] C. Huang, "Improved pseudospectral mode solver by prolate spheroidal wave functions for optical waveguides with step-index," *J. Lightwave Technol.*, vol. 27, no. 5, pp. 597–605, Mar. 2009.

[8] J. Xiao, H. Ma, N. Bai, X. Liu, and X. Sun, "Full-vectorial mode solver for bending waveguides using multidomain pseudospectral method in a cylindrical coordinate system," *IEEE Photon. Technol. Lett.*, vol. 21, no. 23, pp. 1779–1781, Dec. 2009.

[9] J. Xiao and X. Sun, "Full-vectorial mode solver for anisotropic optical waveguides using multidomain spectral collocation method," *Opt. Commun.*, vol. 283, no. 14, pp. 2835–2840, Jul. 2010.

[10] A. Malcolm and D. Nicholls, "A field expansions method for scattering by periodic multilayered media," *J. Acoust. Soc. Amer.*, vol. 129, no. 4, pp. 1783–1793, Apr. 2011.

[11] A. Mastryukov and B. Mikhailenko, "Solving the 2D Maxwell equations by a Laguerre spectral method," *Numer. Anal. Appl.*, vol. 3, no. 2, pp. 118–132, Apr. 2010.

[12] C. Huang, "Semiconductor nanodevice simulation by multidomain spectral method with Chebyshev, prolate spheroidal and Laguerre basis functions," *Comput. Phys. Commun.*, vol. 180, no. 3, pp. 375–383, Mar. 2009.

[13] P. Chiang, C. Yu, and H. Chang, "Analysis of two-dimensional photonic crystals using a multidomain pseudospectral method," *Phys. Rev. E, Stat., Nonlin., Soft Matter Phys.*, vol. 75, no. 2, p. 026703, Feb. 2007.

[14] F. Alharbi, "Predefined exponential basis set for half-bounded multi domain spectral method," *Appl. Math.*, vol. 1, pp. 146–152, Sep. 2010.

[15] D. Chu and G. Golub, "On a generalized eigenvalue problem for nonsquare pencils," *SIAM J. Matrix Anal. Appl.*, vol. 28, no. 3, pp. 770–787, Aug. 2006.

[16] G. Boutry, M. Elad, G. Golub, and P. Milanfar, "The generalized eigenvalue problem for nonsquare pencils using a minimal perturbation approach," *SIAM J. Matrix Anal. Appl.*, vol. 27, no. 2, pp. 582–601, Jan. 2005.

[17] O. Ivanova, M. Hammer, R. Stoffer, and E. van Groesen, "A variational mode expansion mode solver," *Opt. Quantum Electron.*, vol. 39, no. 10/11, pp. 849–864, Aug. 2007.

[18] C. Vassallo, "1993–1995 optical mode solvers," *Opt. Quantum Electron.*, vol. 29, no. 2, pp. 95–114, Feb. 1997.

[19] C. Vassallo and Y. Wang, "A new semirigorous analysis of rib waveguides," *J. Lightwave Technol.*, vol. 8, no. 1, pp. 56–65, Jan. 1990.

[20] G. Hadley and R. Smith, "Full-vector waveguide modeling using an iterative finite-difference method with transparent boundary conditions," *J. Lightwave Technol.*, vol. 13, no. 3, pp. 465–469, Mar. 1995.

[21] M. Koshiba, S. Maruyama, and K. Hirayama, "A vector finite element method with the high-order mixed-interpolation-type triangular elements for optical waveguiding problems," *J. Lightwave Technol.*, vol. 12, no. 3, pp. 495–502, Mar. 1994.

[22] W. Huang and C. Xu, "Simulation of three-dimensional optical waveguides by a full-vector beam propagation method," *IEEE J. Quantum Electron.*, vol. 29, no. 10, pp. 2639–2649, Oct. 1993.
[23] M. Stern, P. Kendall, and P. McIlroy, "Analysis of the spectral index method for vector modes of rib waveguides," *Proc. Inst. Elect. Eng.—J. Optoelectron.*, vol. 137, no. 1, pp. 21–26, Feb. 1990.
[24] S. Sujecki, T. Benson, P. Sewell, and P. Kendall, "Novel vectorial analysis of optical waveguides," *J. Lightwave Technol.*, vol. 16, no. 7, pp. 1329–1335, Jul. 1998.
[25] B. Rahman and J. Davies, "Vector-h finite element solution of gaas/gaalas rib waveguides," *Proc. Inst. Elect. Eng.—J. Optoelectron.*, vol. 132, no. 6, pp. 349–353, Dec. 1985.
[26] J. Xiao and X. Sun, "A modified full-vectorial finite-difference beam propagation method based on *h*-fields for optical waveguides with step-index profiles," *Opt. Commun.*, vol. 266, no. 2, pp. 505–511, Oct. 2006.
[27] A. Sudbo, "Improved formulation of the film mode matching method for mode field calculations in dielectric waveguides," *Pure Appl. Opt., J. Eur. Opt. Soc. A*, vol. 3, no. 3, pp. 381–388, May. 1994.
[28] S. Selleri and J. Petráček, "Modal analysis of rib waveguide through finite element and mode matching methods," *Opt. Quantum Electron.*, vol. 33, no. 4, pp. 373–386, Apr. 2001.
[29] F. Alharbi, "Comparative analysis of spectral methods in half-bounded domains; implementation of predefined exponential and Laguerre basis sets to study planar dielectric and plasmonic waveguides," *Opt. Quantum Electron.*, vol. 41, no. 10, pp. 751–760, Aug. 2009.
[30] P. Lusse, P. Stuwe, J. Schule, and H. Unger, "Analysis of vectorial mode fields in optical waveguides by a new finite difference method," *J. Lightwave Technol.*, vol. 12, no. 3, pp. 487–494, Mar. 1994.
[31] J. Yamauchi, M. Sekiguchi, O. Uchiyama, J. Shibayama, and H. Nakano, "Modified finite-difference formula for the analysis of semivectorial modes in step-index optical waveguides," *IEEE Photon. Technol. Lett.*, vol. 9, no. 7, pp. 961–963, Jul. 1997.
[32] J. Mu, H. Liang, X. Li, B. Xu, and W. Huang, "Vector mode analysis of optical waveguides by quadratic spline collocation method," *Progr. Electromagn. Res. M*, vol. 27, pp. 97–107, 2012.